DØ Note 5038-CONF v2.1

Search for Flavor Changing Neutral Current Charm Decays $D \to \pi^+\mu^+\mu^-$

The DØ Collaboration
URL: http://www-d0.fnal.gov

(Dated: March 9, 2006)

We study the flavor changing neutral current process $c \to u\mu^+\mu^-$ using approximately 1 fb^{-1} of $p\bar{p}$ collisions at $\sqrt{s} = 1.96$ TeV recorded by the DØ detector operating at the Fermilab Tevatron. We observe the $D_s^+ \to \phi\pi^+ \to \pi^+\mu^+\mu^-$ final state with a significance above background greater than 7 standard deviations and see evidence for $D^+ \to \phi\pi^+ \to \pi^+\mu^+\mu^-$ with a significance above background of 3.1 standard deviations. By normalizing to the known $D_s^+ \to \phi\pi^+$ and $\phi \to \mu^+\mu^-$ branching fractions, we measure $\mathcal{B}(D^+ \to \phi\pi^+ \to \pi^+\mu^+\mu^-) = (1.75 \pm 0.7 \pm 0.5) \times 10^{-6}$. We search for continuum production of $D^+ \to \pi^+\mu^+\mu^-$ in the dimuon invariant mass spectrum away from the ϕ resonance. We see no evidence of signal above background in this mode and set a limit of $\mathcal{B}(D^+ \to \pi^+\mu^+\mu^-) < 4.7 \times 10^{-6}$ at the 90% confidence level.

TABLE I: Predictions for both long distance and Standard Model short distance contributions for $D \to \pi$, $K\mu^+\mu^-$ decays taken from Ref. [7].

	Short distance branching fraction	Long distance branching fraction
$D_s^+ \to \pi^+\mu^+\mu^-$	0	6.1×10^{-6}
$D^+ \to \pi^+\mu^+\mu^-$	9.4×10^{-9}	1.0×10^{-6}
$D_s^+ \to K^+\mu^+\mu^-$	9.0×10^{-10}	4.3×10^{-8}
$D^+ \to K^+\mu^+\mu^-$	0	7.1×10^{-9}

Flavor changing neutral current (FCNC) decays are forbidden at tree level in the Standard Model (SM) and proceed via higher order penguin or box diagrams. Many extensions of the SM allow for tree level diagrams or alternative loop diagrams for FCNC that could significantly alter the decay rate with respect to SM expectations. The excellent agreement between observed FCNC processes involving down-type charge $-1/3$ quarks such as $b \to s\gamma$, $b \to sl^+l^-$, and $K \to \pi\nu\bar{\nu}$ with SM expectations have been used to set strict limits on new phenomena [1–3]. However, there are several scenarios of new phenomena such as SUSY R parity violation in a single coupling scheme [3], or little Higgs models with a new up-like vector quark [4] where deviations from the SM would only be seen in the up sector. Scenarios of this nature motivate the study of FCNC charm meson decays.

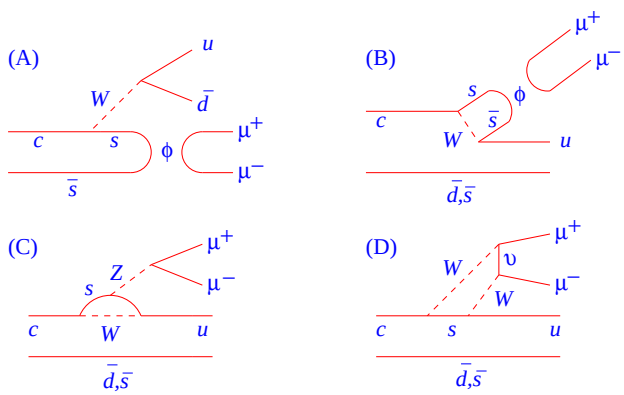

FIG. 1: Feynman diagrams for $D \to \pi^+\mu^+\mu^-$ and $K^+\mu^+\mu^-$. A: Long distance Cabbibo favored $D_s^+ \to \phi\pi^+ \to \pi^+\mu^+\mu^-$. B: Long distance Cabbibo suppressed $D^+ \to \phi\pi^+ \to \pi^+\mu^+\mu^-$ and $D_s^+ \to \phi K^+ \to K^+\mu^+\mu^-$. C: $c \to u$ penguin diagram for $D^+ \to \pi^+\mu^+\mu^-$ and $D_s^+ \to K^+\mu^+\mu^-$. D: $c \to u$ box diagram for $D^+ \to \pi^+\mu^+\mu^-$ and $D_s^+ \to K^+\mu^+\mu^-$. The penguin and box diagrams also proceed via internal b and d quark loops leading to strong GIM suppression of these processes.

Due to GIM suppression, the SM rates for FCNC charm decays vanish in the limit of SU(3) symmetry. The inclusive rates of decays such as $D^+ \to \pi^+l^+l^-$ [5] are therefore expected to be dominated by long distance contributions where the dilepton system is produced via intermediate strong resonances such as the ϕ or the ω [6, 7] as illustrated in Fig. 1. Predictions for the branching fractions of the various channels are given in Table I [7]. Of particular interest is the decay $D_s^+ \to \pi^+\mu^+\mu^-$ that can only proceed via the long distance interaction where the dimuon system is produced by an intermediate ϕ meson. Since this has no short distance contributions, the rate is given simply by the product of the two branching fractions of $D_s^+ \to \phi\pi^+$ and $\phi \to \mu^+\mu^-$. Just as the decay $B^+ \to J/\psi K^+ \to K^+l^+l^-$ played a crucial role in benchmarking the studies of $b \to sl^+l^-$ transitions, the observation of the Cabbibo favored decay $D_s^+ \to \phi\pi^+ \to \pi^+l^+l^-$ is an essential first step in the study of $c \to ul^+l^-$ transitions. Once this mode has been observed, the search for continuum production of $c \to ul^+l^-$ can be performed by looking for an excess of D^+ candidates where the dilepton mass is inconsistent with resonance production.

In this Note we report a study of FCNC charm decays including the observation of the decay $D_s^+ \to \phi\pi^+ \to \pi^+\mu^+\mu^-$ and evidence for the decay $D^+ \to \phi\pi^+ \to \pi^+\mu^+\mu^-$ by requiring a dimuon mass window around the nominal ϕ mass. We then search for $c \to u\mu^+\mu^-$ by looking for an excess in the $D^+ \to \pi^+\mu^+\mu^-$ final state in the continuum region of the dimuon invariant mass spectrum below and above the ϕ resonance. The study uses a data sample of $p\bar{p}$ collisions at $\sqrt{s} = 1.96$ TeV recorded by the DØ detector operating at the Fermilab Tevatron corresponding to a delivered luminosity of approximately 1 fb^{-1}. Similar studies have been performed by other experiments with the most stringent limits on three body FCNC charm decays with dimuons set by FOCUS [8] and with dielectrons set by CLEO-c [9]. These results are summarized in Table II.

TABLE II: 90% confidence level upper limits on $D \to \pi$, Kl^+l^- decays. The dimuon modes are from FOCUS [8] and the dielectron limits are from CLEO-c [9]. The FOCUS limits are on the total rate while the CLEO limits exclude the contribution from $\phi \to e^+e^-$.

	90% C.L. upper limits
$D_s^+ \to \pi^+\mu^+\mu^-$	29×10^{-6}
$D^+ \to \pi^+\mu^+\mu^-$	8.8×10^{-6}
$D_s^+ \to K^+\mu^+\mu^-$	36×10^{-6}
$D^+ \to K^+\mu^+\mu^-$	9.2×10^{-6}
$D^+ \to \pi^+e^+e^-$	7.4×10^{-6}
$D^+ \to K^+e^+e^-$	6.2×10^{-6}

The DØ detector is a general purpose spectrometer and calorimeter [10]. Charged particles are reconstructed using a silicon vertex tracker and a scintillating fiber tracker located inside a superconducting solenoid coil that provides a 2 T magnetic field. Photons and electrons are reconstructed using the inner region of a liquid argon calorimeter optimized for electromagnetic shower detection. Jet reconstruction and electron identification are further augmented with the outer region of the calorimeter optimized for hadronic shower detection. Muons are reconstructed using a spectrometer consisting of magnetized iron toroids and three super-layers of proportional tubes and plastic trigger scintillators located outside the calorimeter.

The DØ trigger is based on a three tier system. The level 1 and 2 dimuon triggers rely on energy deposited in the muon spectrometer and fast reconstruction of muon tracks. The level 3 trigger performs fast reconstruction of the entire event allowing for further muon identification algorithms, matching of muon candidates to tracks reconstructed in the central tracking system, and requirements on the z position of the primary vertex.

The analysis requirements are determined using Pythia [11] Monte Carlo (MC) to model both $c\bar{c}$ and $b\bar{b}$ production and fragmentation. The EvtGen [12] MC is used to decay prompt D mesons and secondary D mesons from B meson decay into the $\phi\pi^+$ and $\pi^+\mu^+\mu^-$ intermediate and final states. The detector response is modeled using a GEANT [13] based MC. The dimuon trigger is modeled using a detailed simulation program incorporating all aspects of the trigger logic. Backgrounds are modeled using data in the mass sideband regions of $1.4 < m(\pi^+\mu^+\mu^-) < 1.6$ GeV/c^2 and $2.2 < m(\pi^+\mu^+\mu^-) < 2.4$ GeV/c^2.

Muon candidates are required to have segments reconstructed in at least two of the muon system super layers and be associated to a track reconstructed with hits in both the silicon and fiber trackers. The muon momentum determined by the muon spectrometer is replaced by the momentum of the associated track. We require the muon transverse momentum p_T be greater than 2 GeV/c and the total momentum p be above 3 GeV/c. The dimuon system is formed by combining two oppositely charged muon candidates that are associated with the same track jet [14] and the same primary vertex, form a well reconstructed vertex, and have an invariant mass $m(\mu^+\mu^-)$ below 2 GeV/c^2. For the initial search for the long distance component to the $\mu^+\mu^-$ system, we require $0.96 < m(\mu^+\mu^-) < 1.06$ GeV/c^2 and redetermine the $\mu^+\mu^-$ momentum with a ϕ mass constraint imposed. The dimuon mass distribution in the region of the ϕ, ω, and ρ resonances is shown in Fig. 2.

Candidate $D^+_{(s)}$ mesons are formed by combining the dimuon system with a track that is associated with the same track jet and primary vertex as the dimuon system, has hits in both the silicon and fiber trackers, and has $p_T > 0.18$ GeV/c. The invariant mass of the three body system must be in the range 1.3 GeV/$c^2 < m(\pi^+\mu^+\mu^-) < 2.5$ GeV/c^2. The three particles must form a well-reconstructed vertex, and the flight direction must be consistent with a particle originating from the primary vertex. In the event of multiple D candidates, the best candidate is chosen based on the $\chi^2_{\rm vtx}$ of the three track vertex, the inverse of the transverse momentum of the pion κ_π in units of (GeV/c)$^{-1}$ and the angular separation between the pion and the dimuon system in η-ϕ space $\Delta R^2_\pi = \Delta\eta^2 + \Delta\phi^2$. We select the candidate with the minimum of

$$\mathcal{M} = \chi^2_{\rm vtx} + \kappa^2_\pi + \Delta R^2_\pi,$$

shown in Fig. 3 for correct and incorrect candidates in MC. The $m(\pi^+\mu^+\mu^-)$ distributions for MC and data after the above selection criteria are shown in Fig. 4.

Backgrounds are reduced using five variables (Fig. 5). The Isolation is defined as $\mathcal{I}_D = p(D)/\sum p_{\rm cone}$ where the sum is over tracks in a cone centered on the D meson of radius $\Delta R = 1$. The transverse flight length significance $\mathcal{S}_D$ defined as the transverse distance of the reconstructed D vertex from the primary vertex normalized to the error in the primary and D vertex measurements. The collinearity angle Θ_D defined as the angle between the D momentum vector and the position vector pointing from the primary to the secondary vertex. The pion impact parameter significance

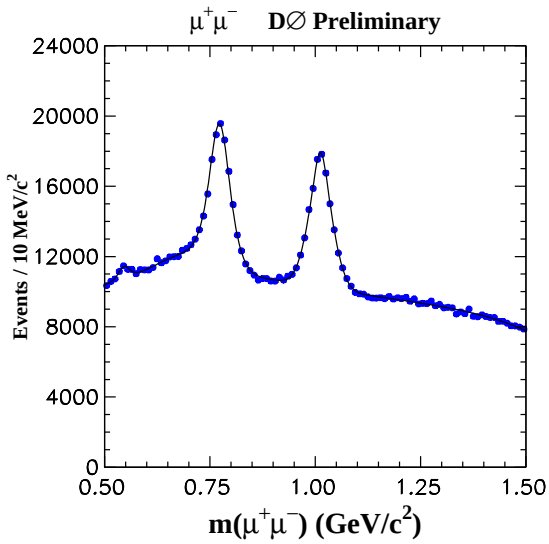

FIG. 2: The inclusive $m(\mu^+\mu^-)$ invariant mass spectrum for the 1 fb^{-1} DØ data sample.

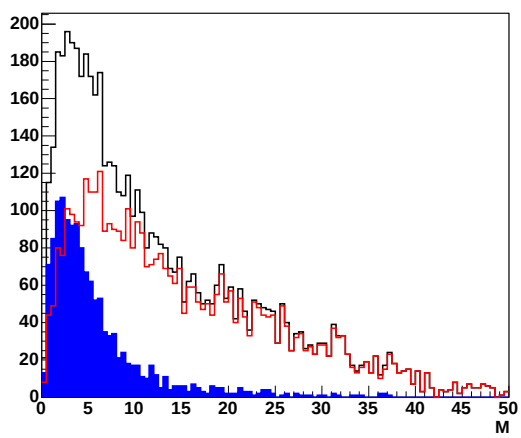

FIG. 3: The $\mathcal{M}$ variable used to select the best candidate per event for MC. The black histogram is all candidates. The solid blue histogram is the correct candidate. The red histogram contains the incorrect candidates.

$\mathcal{S}_\pi$ is the point of closest approach of the pion helix to the interaction point in the transverse plane relative to its error. Finally the variable $\mathcal{M}$ defined above is also used. The variables are displayed in Figures 6 through 10 for both D_s^+ and D^+ signal MC and sideband data.

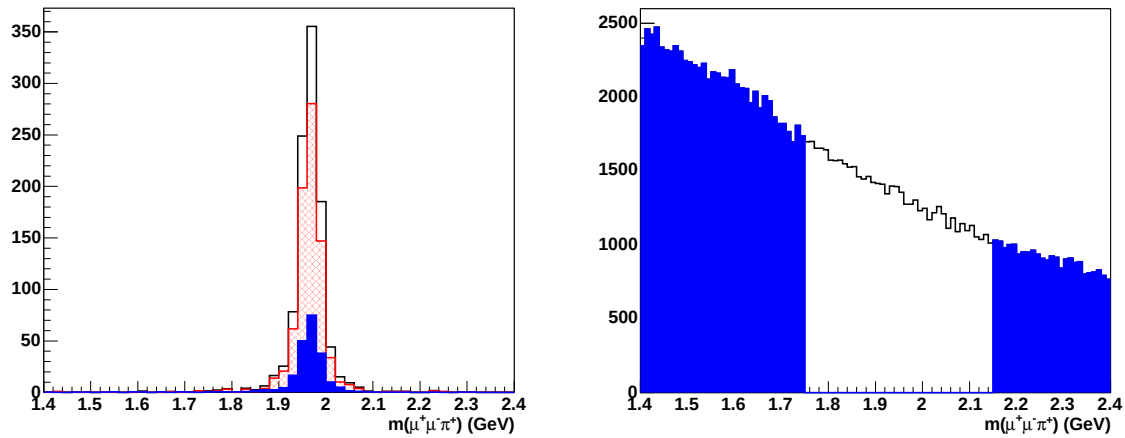

FIG. 4: The $m(\mu^+\mu^-\pi^+)$ distribution for $D_s^+ \to \phi\pi^+ \to \pi^+\mu^+\mu^-$ signal MC (left). The hatched red histogram is the prompt component; the solid blue histogram is the $B \to D_s$ component; the open black histogram is the sum of the two components. The right histogram is the distribution in data after applying the D selection requirements described in the text. The blue solid region signifies the sideband used to model the background for the background suppression variables.

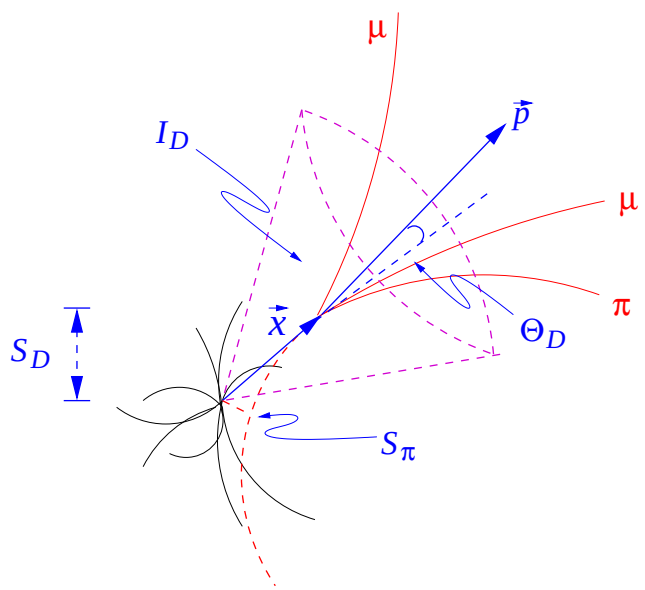

FIG. 5: Representation of the background suppression variables described in the text.

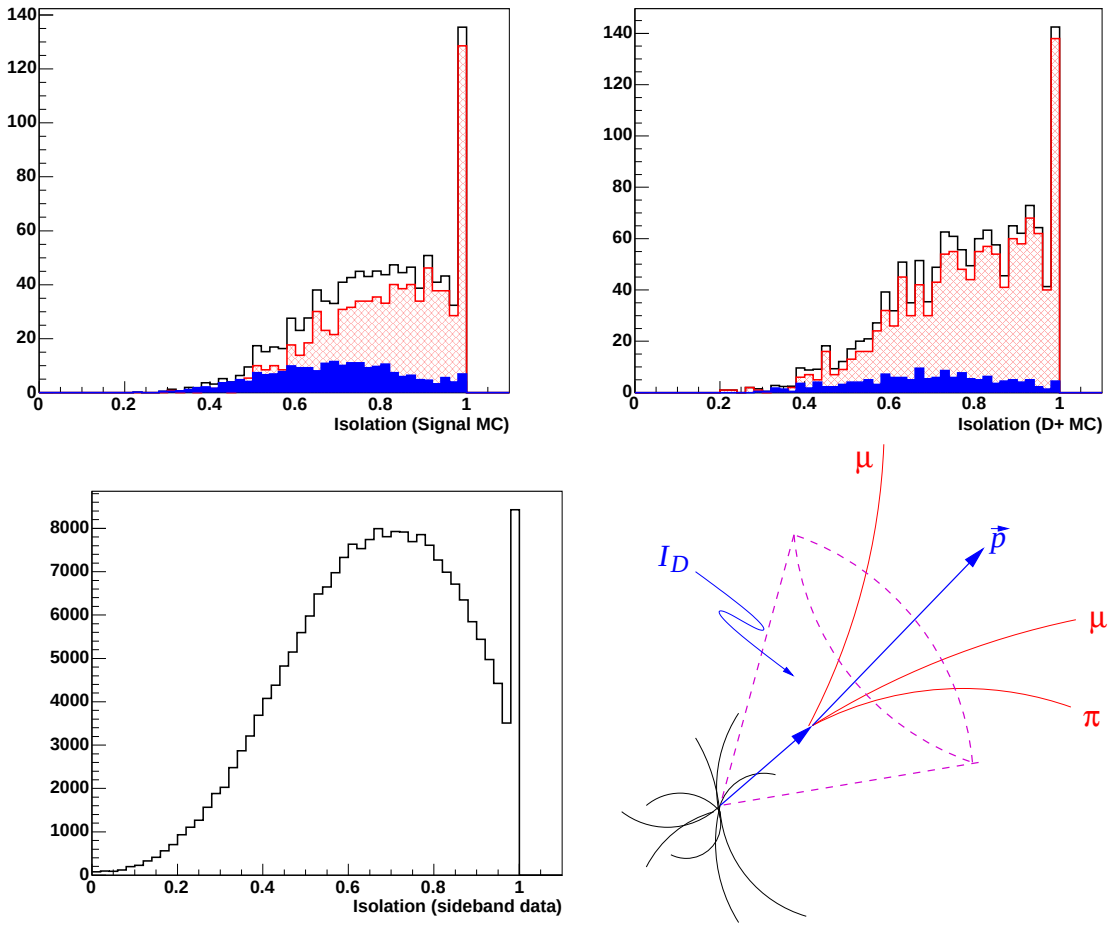

FIG. 6: The isolation variable, $\mathcal{I}_D$. The distribution on the top left is $D_s^+ \to \phi\pi^+ \to \pi^+\mu^+\mu^-$ signal MC. The distribution on the top right is $D^+ \to \phi\pi^+ \to \pi^+\mu^+\mu^-$ signal MC. The hatched red histogram is the prompt component; the solid blue histogram is the $B \to D_s$ component; the open black histogram is the sum of the two components. The distribution on the bottom is D candidates in data in the D mass sideband regions $1.4 < m(\pi^+\mu^+\mu^-) < 1.75$ GeV/c^2 and $2.05 < m(\pi^+\mu^+\mu^-) < 2.4$ GeV/c^2.

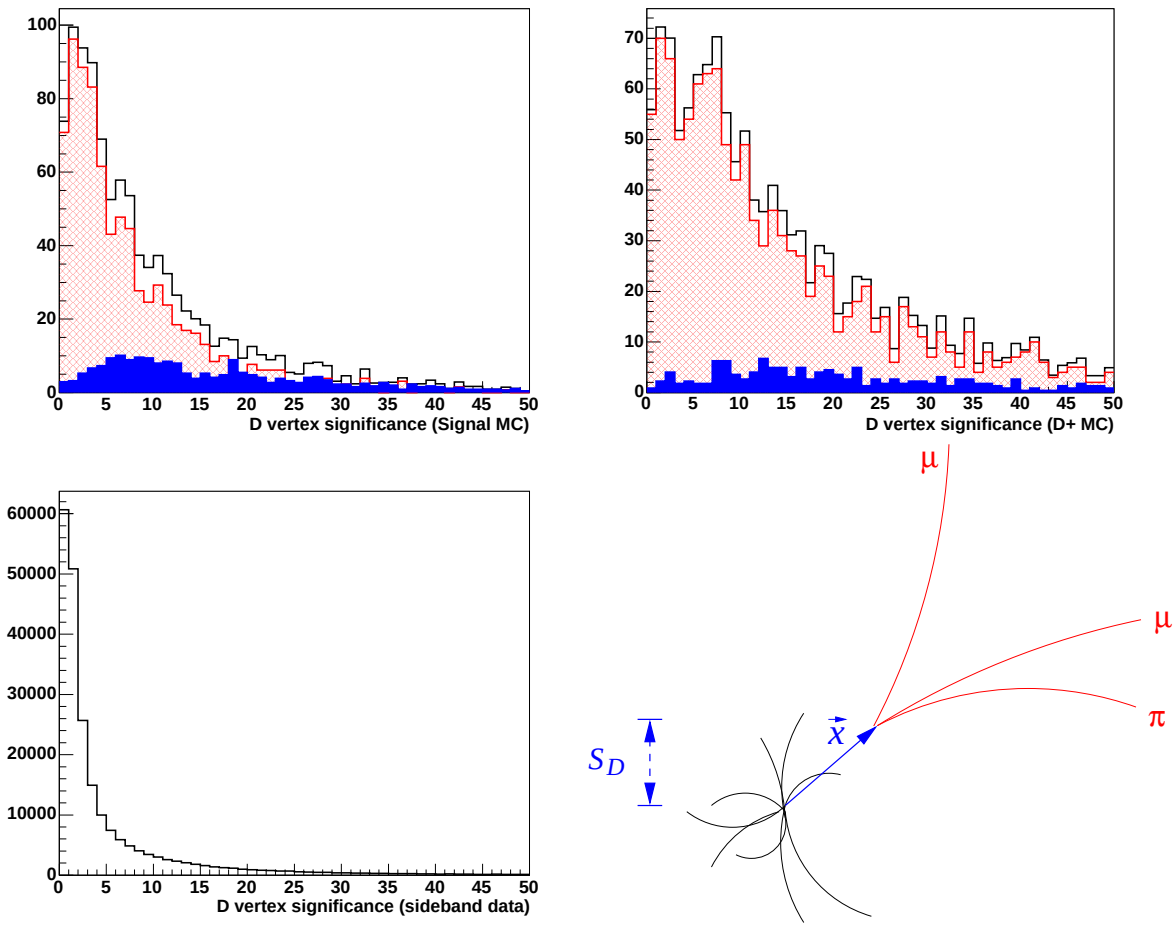

FIG. 7: The significance variable, $\mathcal{S}_D$. The distribution on the top left is $D_s^+ \to \phi\pi^+ \to \pi^+\mu^+\mu^-$ signal MC. The distribution on the top right is $D^+ \to \phi\pi^+ \to \pi^+\mu^+\mu^-$ signal MC. The hatched red histogram is the prompt component; the solid blue histogram is the $B \to D_s$ component; the open black histogram is the sum of the two components. The distribution on the bottom is D candidates in data in the D mass sideband regions $1.4 < m(\pi^+\mu^+\mu^-) < 1.75$ GeV/c^2 and $2.05 < m(\pi^+\mu^+\mu^-) < 2.4$ GeV/c^2.

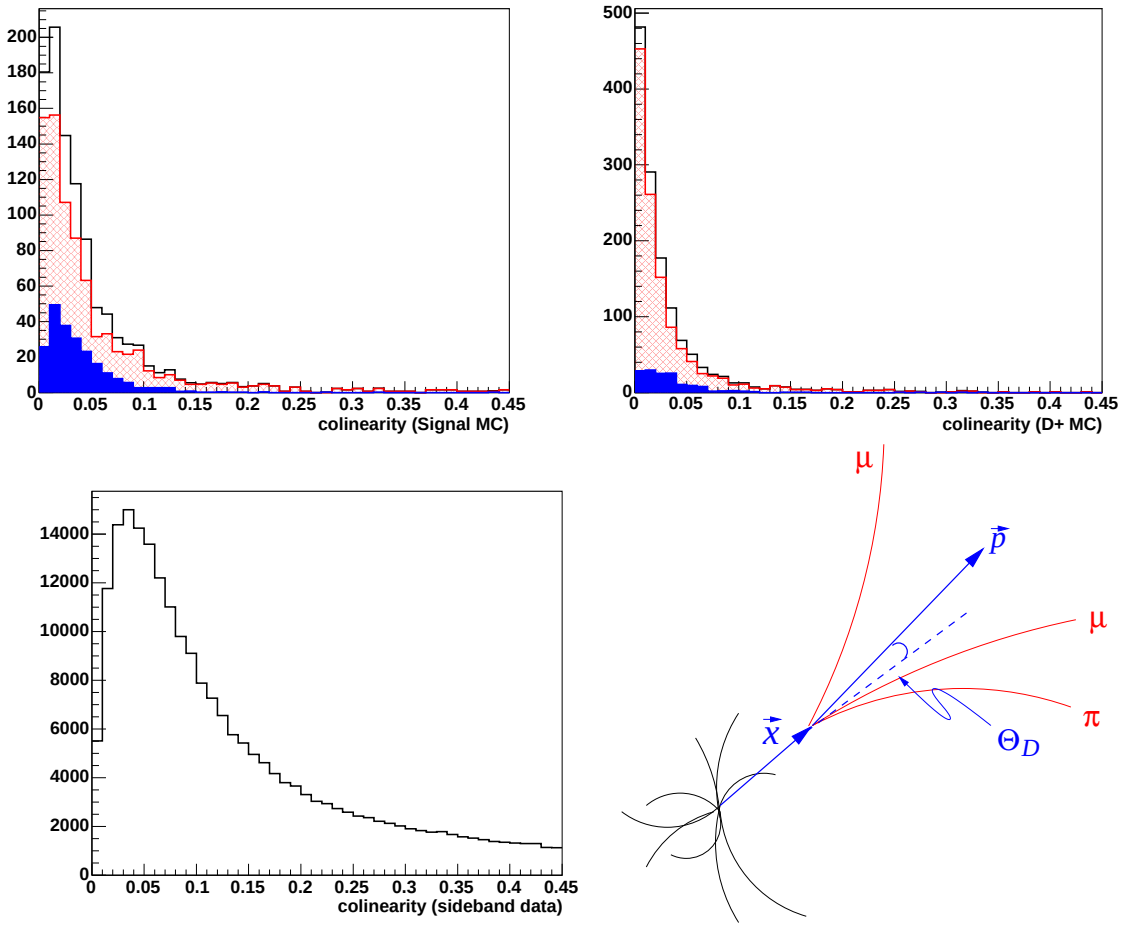

FIG. 8: The collinearity angle variable, Θ_D. The distribution on the top left is $D_s^+ \to \phi\pi^+ \to \pi^+\mu^+\mu^-$ signal MC. The distribution on the top right is $D^+ \to \phi\pi^+ \to \pi^+\mu^+\mu^-$ signal MC. The hatched red histogram is the prompt component; the solid blue histogram is the $B \to D_s$ component; the open black histogram is the sum of the two components. The distribution on the bottom is D candidates in data sample in the D mass sideband regions $1.4 < m(\pi^+\mu^+\mu^-) < 1.75$ GeV/c^2 and $2.05 < m(\pi^+\mu^+\mu^-) < 2.4$ GeV/c^2.

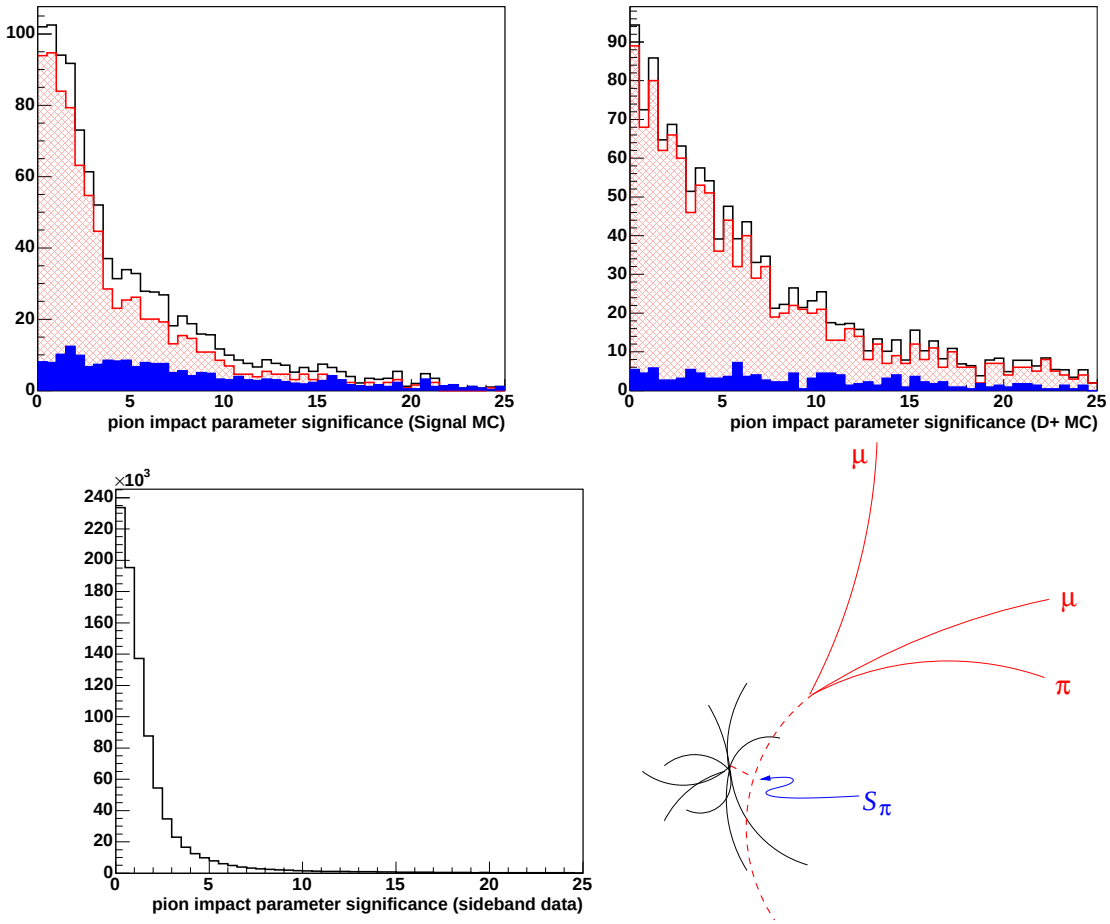

FIG. 9: The pion impact parameter significance variable, $\mathcal{S}_\pi$. The distribution on the top left is $D_s^+ \to \phi\pi^+ \to \pi^+\mu^+\mu^-$ signal MC. The distribution on the top right is $D^+ \to \phi\pi^+ \to \pi^+\mu^+\mu^-$ signal MC. The hatched red histogram is the prompt component; the solid blue histogram is the $B \to D_s$ component; the open black histogram is the sum of the two components. The distribution on the bottom is D candidates in data in the D mass sideband regions $1.4 < m(\pi^+\mu^+\mu^-) < 1.75$ GeV/c^2 and $2.05 < m(\pi^+\mu^+\mu^-) < 2.4$ GeV/c^2.

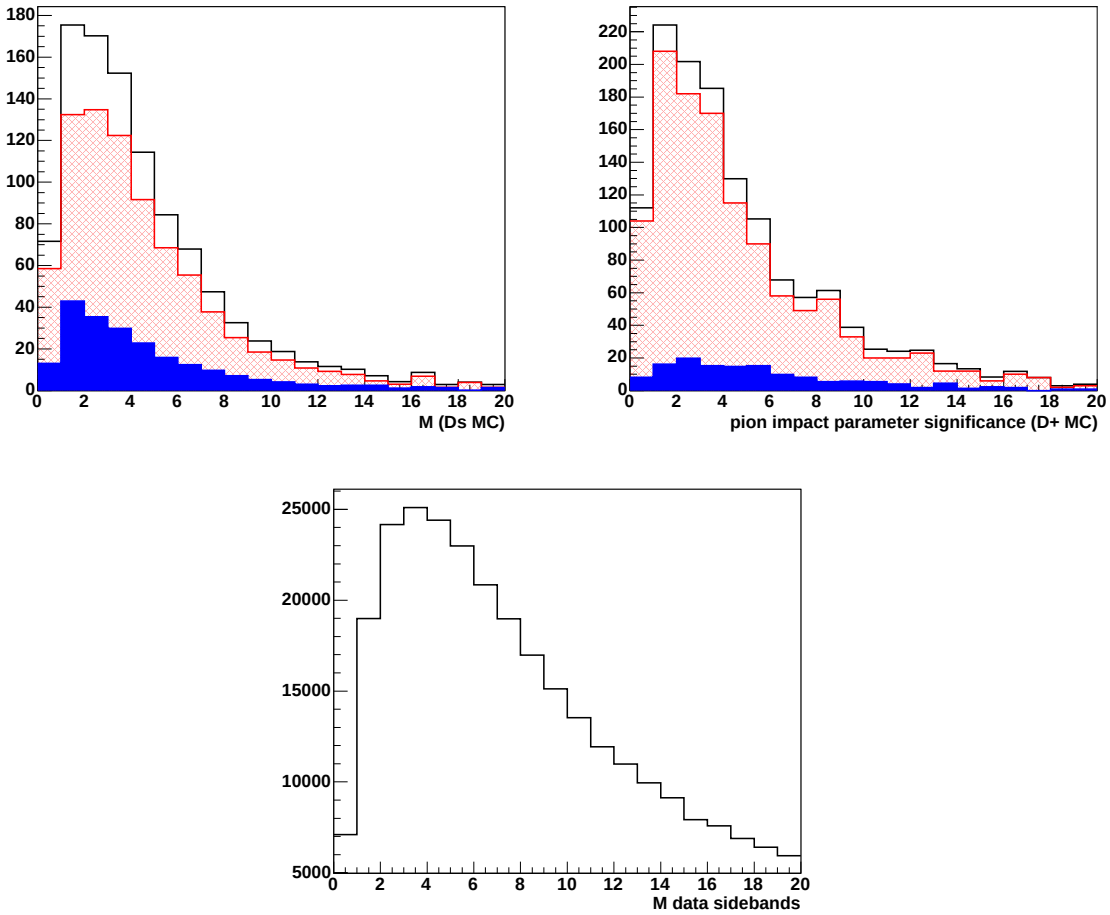

FIG. 10: The $\mathcal{M}$ variable. The distribution on the top left is $D_s^+ \to \phi\pi^+ \to \pi^+\mu^+\mu^-$ signal MC. The distribution on the top right is $D^+ \to \phi\pi^+ \to \pi^+\mu^+\mu^-$ signal MC. The hatched red histogram is the prompt component; the solid blue histogram is the $B \to D_s$ component; the open black histogram is the sum of the two components. The distribution on the bottom is D candidates in data sample in the D mass sideband regions $1.4 < m(\pi^+\mu^+\mu^-) < 1.75$ GeV/c^2 and $2.05 < m(\pi^+\mu^+\mu^-) < 2.4$ GeV/c^2.

TABLE III: Loose and optimized cut values for the background suppression variables.

	loose	optimal D_s^+ cut value	optimal D^+ cut value
$\mathcal{I}_D$	> 0.4	> 0.44	> 0.71
$\mathcal{S}_D$	> 3	> 3.4	> 9.4
Θ_D	< 50 mrad	< 32 mrad	< 7 mrad
$\mathcal{S}_\pi$	> 0.5	> 0.57	> 1.8
$\mathcal{M}$	none	< 6.1	< 2.6

We first require the following criteria that we define as our loose selection: $\Theta_D < 50$ mrad, $\mathcal{S}_D > 3$, $\mathcal{S}_\pi > 0.5$, and $\mathcal{I}_D > 0.4$. The $\pi^+\mu^+\mu^-$ invariant mass distribution for the loose selection sample in the window $0.96 < m(\mu^+\mu^-) < 1.06$ GeV/c^2 is shown in Fig 11. The $D^+_{(s)} \to \phi\pi^+ \to \pi^+\mu^+\mu^-$ signal is extracted from a binned likelihood fit to the data assuming possible contributions from D_s^+ and D^+ initial states as signal and combinatoric background. The signal distributions are modeled as Gaussians. The mean and sigma of the D_s^+ Gaussian are free parameters. The difference in the means of the D_s^+ and D^+ Gaussians are constrained to the known mass difference [15] and the sigmas are constrained by $\sigma(D^+) = (m(D^+)/m(D_s^+)) \times \sigma(D_s^+)$. The background is modeled as an exponential. The fit yields 133 ± 25 D_s^+ candidates at a significance above background of 7.5 standard deviations and 37 ± 19 D^+ candidates at a significance above background of 2.1 standard deviations.

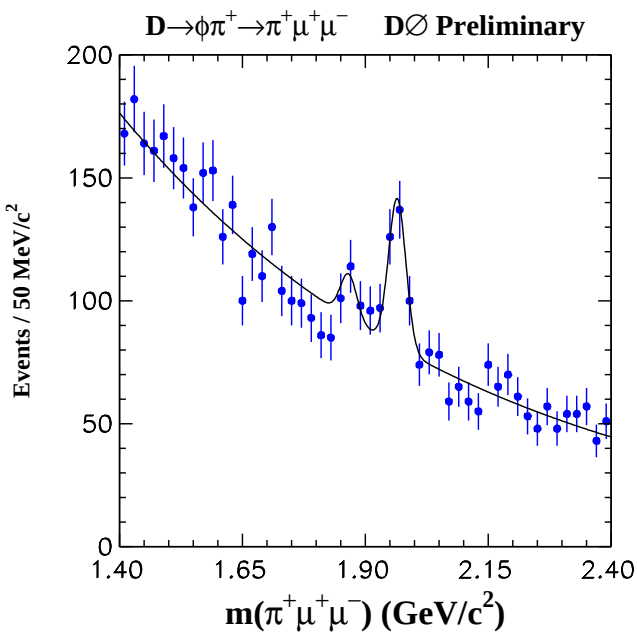

FIG. 11: The $m(\pi^+\mu^+\mu^-)$ mass spectrum for the loose cut sample in the $0.96 < m(\mu^+\mu^-) < 1.06$ GeV/c^2 bin. The results of binned likelihood fits to the distributions including contributions for D_s^+, D^+, and combinatoric background are overlaid on the histogram.

To further optimize the requirements on the background suppression variables, we perform a random grid search [16] using the five variables discussed above: $\mathcal{M}$, $\mathcal{I}_D$, $\mathcal{S}_D$, Θ_D, and $\mathcal{S}_\pi$. The signal is modeled using MC and the background is modeled using sideband data. The final cuts are chosen to maximize $\epsilon/(a/2 + \sqrt{N_{bkg}})$ [17] where ϵ is the signal efficiency relative to the loose cut selection, N_{bkg} is the expected number of background events based on a sideband to signal box scale factor determined from the fit to the loose cut $m(\pi^+\mu^+\mu^-)$ distribution, and a is 1.64 chosen to optimize selection for 90% confidence level upper limits. The optimization is performed separately for D^+ and D_s^+ MC. The longer lifetime of the D^+ allows us to make tighter requirements on the suppression variables while maintaining adequate signal efficiency. We refer to the requirements determined using D_s^+ MC as the optimized D_s^+ selection and the requirements using the D^+ MC as the optimized D^+ selection. The final requirements are listed in Table III.

TABLE IV: Efficiency ratio and associated relative systematic errors for the D_s^+ and D^+ to $\phi\pi^+$ modes.

ϵ^+/ϵ^s	1.19
D p_T modeling	+0.4%
resolution scale	+1%, −3%
multiplicity	−10%
luminosity	+13%,
total	+13%, −10%

The $m(\pi^+\mu^+\mu^-)$ distribution after applying the optimized D_s^+ selection in the $0.96 < m(\mu^+\mu^-) < 1.06$ GeV/c^2 bin is shown in Fig. 12. The parameters of the Gaussians are fixed to the values determined in the fit to the loose sample and the background slope and normalization are free parameters. The fit yields 65 ± 11 D_s^+ events and 26 ± 9 D^+ events with a significance above background of 3.1 standard deviations determined by the change in the fit likelihood with the nominal D^+ yield and the fit without a D^+ component.

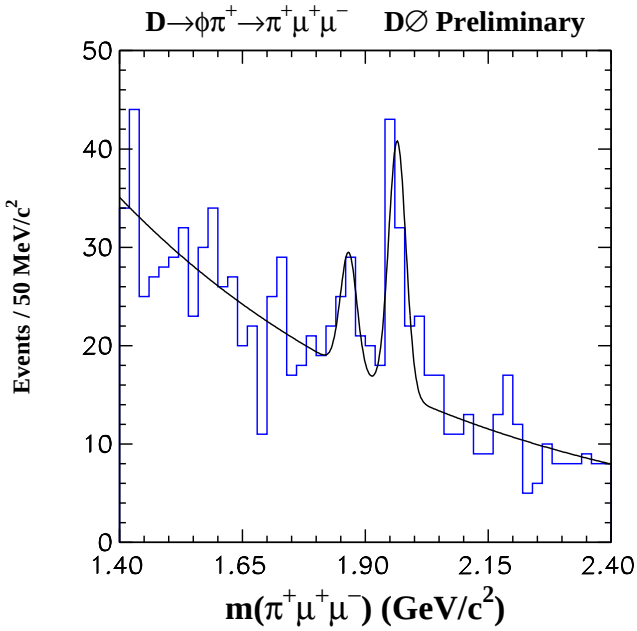

FIG. 12: The $m(\pi^+\mu^+\mu^-)$ mass spectrum for the optimized D_s^+ sample in the $0.96 < m(\mu^+\mu^-) < 1.06$ GeV/c^2 bin. The results of binned likelihood fits to the distributions including contributions for D_s^+, D^+, and combinatoric background are overlaid on the histogram.

The relative efficiency between the D_s^+ and D^+ modes is taken from MC. Systematic biases are possible due to improper modeling of the D meson p_T distribution, improper modeling of the charged particle multiplicity in the interaction, improper modeling of multiple interactions, and improper modeling of the impact parameter resolutions. Systematic errors for these effects are derived by comparing the MC distributions to the distributions in data in the loose sample. The efficiency ratio and associated systematic errors between the D^+ and D_s^+ signals for the optimized D_s^+ cuts are listed in Table IV.

The efficiency is determined separately for prompt D mesons and D mesons from B decay and combined using the measured prompt fractions [18]:

$$\epsilon^+ = f_p^+ \epsilon^+_{\rm prompt} + (1 - f_p^+)\epsilon^+_{B\to D}$$

where $\epsilon^+_{\rm prompt}$ is the efficiency for prompt D^+ mesons, $\epsilon^+_{B\to D}$ is the efficiency for D mesons from B decay, and f_p^+ is the fraction of prompt D^+ mesons. We write an equivalent expression for D_s^+ mesons by replacing the + superscript

TABLE V: External inputs to the efficiency calculation.

f_p^+ [18]	0.891 ± 0.004
f_p^s [18]	0.773 ± 0.038
$f_{c\to D}^+$ [19]	0.232 ± 0.018
$f_{c\to D}^s$ [19]	0.101 ± 0.027

with an s. The yield ratio is related to the ratio of branching fractions by

$$\frac{n(D^+)}{n(D_s)} = \frac{f_{c\to D}^+}{f_{c\to D}^s} \times \frac{f_p^s}{f_p^+} \times \frac{\epsilon^+}{\epsilon^s} \times \frac{\mathcal{B}(D^+ \to \phi\pi^+ \to \pi^+\mu^+\mu^-)}{\mathcal{B}(D_s \to \phi\pi^+) \times \mathcal{B}(\phi \to \mu^+\mu^-)},$$

where $f_{c\to D}^+$ is the fraction of D^+ mesons produced in c quark fragmentation and $f_{c\to D}^s$ is the equivalent fraction for D_s^+ mesons [19]. The production and prompt fractions are listed in Table V. The D^+ branching fraction is then given by

$$\mathcal{B}(D^+ \to \phi\pi^+ \to \pi^+\mu^+\mu^-) = \frac{n(D^+)}{n(D_s)} \times \frac{f_{c\to D}^s}{f_{c\to D}^+} \times \frac{f_p^+}{f_p^s} \times \frac{\epsilon^s}{\epsilon^+} \times \mathcal{B}(D_s \to \phi\pi^+) \times \mathcal{B}(\phi \to \mu^+\mu^-).$$

Using the efficiency ratio and production fractions, the ratio of branching fractions of D^+ to D_s^+ is given by

$$\frac{\mathcal{B}(D^+ \to \phi\pi^+ \to \pi^+\mu^+\mu^-)}{\mathcal{B}(D_s^+ \to \phi\pi^+) \times \mathcal{B}(\phi \to \mu^+\mu^-)} = 0.17 \pm 0.07 \pm 0.05$$

where the first error is statistics and the second is the combined systematics. Using the central value of $D_s^+ \to \phi\pi^+$ and $\phi \to \mu^+\mu^-$ branching fractions gives

$$\mathcal{B}(D^+ \to \phi\pi^+ \to \pi^+\mu^+\mu^-) = (1.75 \pm 0.7 \pm 0.5) \times 10^{-6}$$

which can be compared to the recent CLEO-c measurement of $(2.7^{+3.6}_{-1.8} \pm 0.2) \times 10^{-6}$ or the expected value of 1.77×10^{-6} given by the product of the $D^+ \to \phi\pi^+$ and the $\phi \to \mu^+\mu^-$ branching fractions.

We now turn to the search for continuum production of $D^+ \to \pi^+\mu^+\mu^-$. To verify that we have not over tuned the background suppression requirements, we examine the $m(\pi^+\mu^+\mu^-)$ distribution after applying the optimized D^+ selection in the $0.96 < m(\mu^+\mu^-) < 1.06$ GeV/c^2 bin, shown in Fig. 13. The background in the signal region is determined by fitting the distribution with a flat offset excluding the signal regions of 1.816 to 1.910 GeV/c^2 for the D^+ and 1.910 to 2.017 GeV/c^2 for the D_s^+. These are the $\pm 3\sigma$ regions determined from the fit to the loose sample. There are 6 events in the D^+ window with estimated backgrounds of 1.06 ± 0.35 events from combinatoric background and 0.14 ± 0.02 feed down events from $D_s^+ \to \phi\pi^+$ giving an excess of 4.8 ± 0.35 We see 3 events in the D_s^+ window with a background of 1.20 ± 0.40 events or an excess of 1.8 ± 0.4. Using the relative efficiency for the D^+ and D_s^+ cuts and the yields in the optimized D_s^+ sample (Fig. 12) we expect 4.1 ± 1.5 D^+ candidates and 3.4 ± 0.6 D_s^+ candidates indicating good agreement between the MC model and the actual efficiency in data.

The $\pi^+\mu^+\mu^-$ invariant mass distribution in data for the entire dimuon invariant mass region excluding $0.96 < m(\mu^+\mu^-) < 1.06$ is shown in Fig 14. The D^+ signal region contains 17 events and the combinatoric background determine from the sidebands is 20.9 ± 3.4. The probability of a background fluctuation is 23%.

The efficiency between the $D^+ \to \pi^+\mu^+\mu^-$ and $D_s^+ \to \phi\pi^+$ samples is given in Table VI including the systematics defined above. Using this, we find

$$\frac{\mathcal{B}(D^+ \to \pi^+\mu^+\mu^-)}{\mathcal{B}(D_s^+ \to \phi\pi^+) \times \mathcal{B}(\phi \to \mu^+\mu^-)} < 0.46 \;\; 90\% \text{ CL}.$$

Using the central value of $D_s^+ \to \phi\pi^+$ and $\phi \to \mu^+\mu^-$ branching fractions gives

$$\mathcal{B}(D^+ \to \pi^+\mu^+\mu^-) < 4.7 \times 10^{-6} \;\; 90\% \text{ CL}.$$

which can be compared to the recent CLEO-c limit in the dielectron channel of 7.4×10^{-6} or the FOCUS limit of 8.8×10^{-6}.

In conclusion, we have performed a detailed study of D_s^+ and D^+ decays to the $\pi^+\mu^+\mu^-$ final states. We clearly observe the $D_s^+ \to \phi\pi^+$ intermediate state and see evidence for the $D^+ \to \phi\pi^+$ intermediate state. The branching

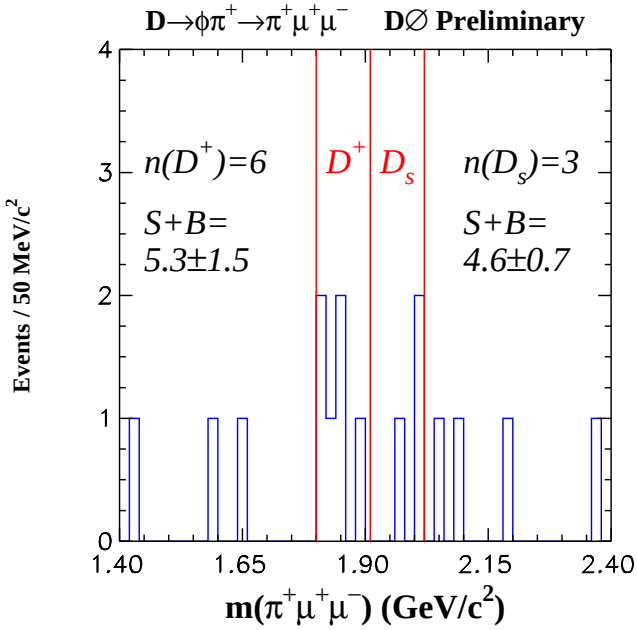

FIG. 13: The $m(\pi^+\mu^+\mu^-)$ mass spectrum for the optimized D^+ sample in the $0.96 < m(\mu^+\mu^-) < 1.06$ GeV/c^2 bin. The line is a fit to the data in the sideband regions $1.4 < m(\pi^+\mu^+\mu^-) < 1.7$ GeV/c^2 and $2.1 < m(\pi^+\mu^+\mu^-) < 2.4$ GeV/c^2. The D^+ and D_s^+ signal yields are fixed based on the yields in the optimized D_s^+ sample and the relative efficiencies between the D_s^+ and D^+ cuts.

TABLE VI: Efficiency ratio and associated systematic errors for the D_s^+ and D^+ to $\phi\pi^+$ modes.

ϵ^+/ϵ^s	0.27
p_T weighting	+7%
resolution scale	+3%, −2%
multiplicity	+9%
luminosity	−9%
total	+12%, −9%

fraction for the $D^+ \to \phi\pi^+ \to \pi^+\mu^+\mu^-$ final state is consistent with the product of $D^+ \to \phi\pi^+$ and $\phi \to \mu^+\mu^-$ branching fractions. We have performed a search for continuum production of $D^+ \to \pi^+\mu^+\mu^-$ by excluding the region of the dimuon invariant mass spectrum around the ϕ. We see no evidence of signal above background and set a limit of $\mathcal{B}(D^+ \to \pi^+\mu^+\mu^-) < 4.7 \times 10^{-6}$ at the 90% confidence level. This is the most stringent limit to date in these modes. Although this is approximatly 500 times above the SM expected signal it is already below the allowed parameter space of SUSY R parity violating couplings. However it is still an order of magnitude above the expected level from little Higgs models.

We thank the staffs at Fermilab and collaborating institutions, and acknowledge support from the Department of Energy and National Science Foundation (USA), Commissariat à L'Energie Atomique and CNRS/Institut National de Physique Nucléaire et de Physique des Particules (France), Ministry for Science and Technology and Ministry for Atomic Energy (Russia), CAPES, CNPq and FAPERJ (Brazil), Departments of Atomic Energy and Science and Education (India), Colciencias (Colombia), CONACyT (Mexico), Ministry of Education and KOSEF (Korea), CONICET and UBACyT (Argentina), The Foundation for Fundamental Research on Matter (The Netherlands), PPARC (United Kingdom), Ministry of Education (Czech Republic), A.P. Sloan Foundation, Civilian Research and Development Foundation, Research Corporation, Texas Advanced Research Program, and the Alexander von Humboldt Foundation.

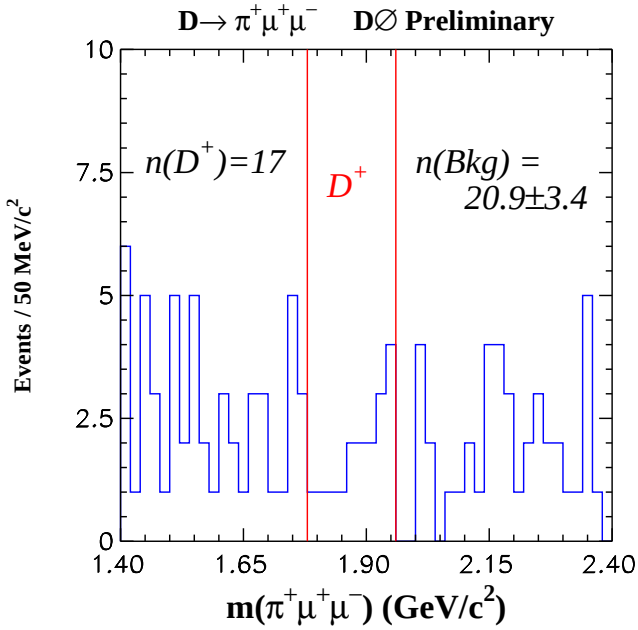

FIG. 14: Final search for $D^+ \to \pi^+\mu^+\mu^-$ in the continuum region.

[1] A.L. Kagen and M. Neubert, Eur. Phys. J. C**7**, 5 (1999).
[2] A. Ali, E. Lunghi, C. Greb, G. Hiller, Phys. Rev. D**66**, 034002 (2002).
[3] K. Agashe and M. Graesser, Phys. Rev. D**54**, 4445 (1996).
[4] S. Fajfer and S. Perlovsek, hep-ph/0511048
[5] The inclusion of charge conjugate modes is implied throughout the text.
[6] G. Burdman, E. Golowich, J. Hewett, S. Pakvasa, Phys. Rev. D**66**, 014009 (2002).
[7] S. Fajfer, S. Prelovsek , P. Singer, Phys. Rev. D**64**, 114009 (2001).
[8] J. M. Link *et al.*, (FOCUS Collaboration), Phys. Lett. B**572**, 21 (2003).
[9] Q. He *et al.*, (CLEO Collaboration) Phys. Rev. Lett. 95, 221802 (2005).
[10] V.M. Abazov *et al.*, (DØ Collaboration) Fermilab-Pub-05/341-E, hep-physics/0507191, submitted to NIM-A.
[11] T. Sjostrand, P. Eden, C. Friberg, L. Lonnblad, G. Miu, S. Mrenna and E. Norrbin, Computer Phys. Commun. 135, 238 (2001).
[12] D. J. Lange, Nuc. Inst. Meth. A**462**, 152 (2001).
[13] R. Brun, F. Bruyant, M. Maire, A. C. McPherson, P. Zanarini, CERN DD/EE/84-1 (1987).
[14] All charged particles in the event are clustered into jets using the DURHAM clustering algorithm with the p_T cut-off parameter 15 GeV/c. S. Catani, Yu. L .Dokshitzer, M. Olsson, G. Turnock, B.R. Webber, Phys.Lett. **B269**, 432 (1991).
[15] S. Eidelman *et al.*, (Particle Data Group), Phys. Lett. **B592**, 1 (2004).
[16] H. B. Prosper, Proceedings CHEP95.
[17] G. Punzi, Proceedings Phystat 2003, physics/0308063.
[18] D. Acosta *et al.*, (CDF Collaboration), Phys. Rev. Lett. **91**, 241804 (2003).
[19] L. Gladilin, hep-ex/9912064 (1999).